Available online at www.sciencedirect.com

SciVerse ScienceDirect

Ceramics International 38 (2012) 2411–2420

CERAMICS INTERNATIONAL

www.elsevier.com/locate/ceramint

A general formulation for strength prediction of advanced ceramics by ball-on-three-balls (B3B)-test with different multiaxial failure criteria

Serkan Nohut *

Zirve University, Faculty of Engineering, Kizilhisar Kampusu, 27260 Gaziantep, Turkey

Received 13 June 2011; received in revised form 1 November 2011; accepted 3 November 2011
Available online 9 November 2011

Abstract

The determination of biaxial strength of ceramics plays a large role in the design of ceramic components. The ball-on-three-balls (B3B)-test is one of the most useful methods for measuring the biaxial strength of ceramics. The strength measured by B3B-test, with any specimen, is dependent on the size of the specimen and loading conditions (type and position of loading); therefore, the strength value, measured with a set of specimens, has to be adjusted by effective volume and/or surface. The standardized strength value obtained from this adjustment can be then used for the design process. Consequently, there is a need for calculating the effective volume/surface of the B3B-test specimens. In this article, general fitting functions are provided for effective volume/surface of B3B-test specimens with different multiaxial criteria, these can be used for all ceramic materials and for various test configurations. Verification of numerical effective volume and effective surface values with experimental measurements show that B3B specimens fail due to surface flaws according to normal stress criterion (NSC).

Keywords: B. Failure analysis; C. Mechanical properties; C. Strength; D. Si_3N_4; B3B-test

1. Introduction

Due to their brittle nature, ceramics show different fracture behavior from that of metals and polymers. Consequently, ceramic engineers need to be aware of this behavior when designing ceramic components for reliable use. A design challenge for the reliable use of ceramic materials in technical applications is the estimation of their failure probability under prescribed boundary- and loading conditions [1,2]. In order to predict the failure probability of advanced ceramics, the fracture of ceramics should be first has to be analyzed with details. Fracture behavior of ceramics can be determined through suitable mechanical tests associated to materials and their applications. Therefore, mechanical tests used for strength measurement plays a significant role in ceramic science-and technology. For metals, strength values measured by any testing method can be directly used for the evaluation of the structural performance. However, for ceramics the measured strength data has to be placed into a context via knowledge of strength testing method and failure mechanism.

In conventional strength tests (e.g. tension test and bending test), ceramic specimens fail under simple stress conditions (i.e. uniaxial stresses). However, in most of the service conditions, a biaxial stress state occurs. Therefore it would be more reliable to use tests which apply biaxial stress state on the specimen since biaxial stress states are known to be more crack sensitive than uniaxial stress states. Dortmans and With [3] compared the results of uniaxial tests (three- and four point bending tests) and biaxial tests (ball-on-ring and ring-on-ring) and stated that in order to determine the best applicable mixed-mode fracture criterion, a varying degree of stress multiaxiality is required for the strength measuring test.

Biaxial test methods provide testing of a larger surface area and/or volume and therefore more critical defects (e.g. defect which lay in different orientations) can be taken into consideration for the failure analysis. Ease of test specimen preparation and ability to test thin sheet materials are other advantages of biaxial tests compared with uniaxial tests. Many studies have been carried out on various biaxial tests. The most commonly used test methods are ring-on-ring test [4–6], sphere-on-ring test [7], ball-on-ring test [8], Brazilian disc test

* Tel.: +90 0342 211 6789; fax: +90 0342 211 6677.
E-mail address: serkan.nohut@zirve.edu.tr.

0272-8842/$36.00
doi:10.1016/j.ceramint.2011.11.007

[9], ring of balls-on-ring of balls test [10], ball-on-three-balls test [11–19] and 3-balls-on-3-balls test [20].

In this study, the ball-on-three-balls (B3B)-test is analyzed. B3B-test is relatively more tolerant of measurement of inaccuracies (e.g. anti-flatness of the surface of the specimen and alignment of the specimen) [11,12]. Edges have no influence of the test results and therefore it is possible to test mini specimens [19]. Precise analytical approximation for the maximum tensile stress in the loaded B3B-test discs is difficult to determine. Thereof, Börger et al. [11] performed a numerical parametric study and provided a general formulation for the prediction of maximum tensile stress in the loaded ceramic disc. Börger et al. [12] investigated the influence of friction between the balls and the disc and they reported that in the numerical simulations, the effect of friction can be neglected. Jeong et al. [13] studied the fracture behavior of alumina ceramics by using the B3B test. The polished surfaces of the discs were indented at different positions distant from the specimen center. They observed a relationship between biaxial strength indenter positions and concluded, for some cases; tangential stresses cause fractures rather than radial stresses. Alumina discs and small rectangular specimens cut from the alumina discs were examined by the B3B test and the same results were obtained from the discs and the rectangular specimens [14]. More than 100 bending tests and approximately 500 B3B tests were performed by Danzer et al. [15] with specimens of zinc oxide varistor, silicon nitride and alumina of different sizes. They reported that the B3B-test is an appropriate method for the strength prediction of brittle materials. Experiments with silicon nitride samples revealed that in the case of small specimens, the strength is much lower than the value predicted by Weibull theory. This shows the importance of the influence of sample size on B3B-test results.

The strength, measured directly from the B3B-test, is dependent on the size of the specimen and configuration of loading and supporting balls. Therefore, the measured strength is case (type of strength measuring test) dependent. However, for the failure probability calculation, the standardized material strength, independent of specimen size and loading configuration, should be used. The standardized material strength can be calculated by normalizing the experimentally measured strength by effective volume and/or effective surface. This demonstrates the importance of the computation of effective volume/surface of the investigated test specimens. Although the maximum tensile stress value is formulated as a function of load and geometric dimensions [11], there is no general formulation for the prediction of effective volume/surface of B3B-test specimens. Only a few studies were found in which effective volume/surface values were determined for some specific sample dimensions with a specific failure criterion [14,15,19].

During the failure probability computation of ceramic components, it is important to know how the normal stresses and shear stresses affect the fracture. Under service conditions, the cracks exist at different positions and lay along different orientations, they are, as a result, subjected to Mode-I as well as Mode-II and Mode-III loading. Therefore, a multiaxial failure criterion is used for the prediction of strength and failure probability [21]. A variety of criteria have been proposed but, due to insufficient information about the crack extension mechanism, it is still not clear which of these criteria is the most appropriate for ceramic materials [22–24]. The opinions of researchers are divided; some say shear stresses have to be taken into account, but others claim that shear-insensitive criteria give better correlation between the numerical and experimental results.

The main purpose of this study is to propose general effective volume and effective surface formulations of B3B-test specimens which is valid for all ceramic materials of different dimensions. Normal stress criterion (NSC), maximum principal stress criterion (MPS) and empirical criterion of Richard (ECR) are used as multiaxial failure criteria. The proposed functions will be verified with the experimental results performed with Si_3N_4 disks and the most appropriate multiaxial failure criterion for Si_3N_4 will be discussed.

2. Experimental procedure

In Fig. 1(a), a sketch of the experimental setup of the general B3B-test is represented [16]. Guides (5) are used to position the specimen (4) and the loading ball (3) which is placed on a stamp (6). The specimen is sustained by the supporting balls (2) and the loading is applied by a punch (1). A preload is performed in order to prevent the balls from slipping [19] and after the preloading, the blocks (7) are removed and the guides are pushed down. The ball configuration is shown in Fig. 1(b). The loading ball touches the disc, with radius R, on the center of the compressive side. The supporting balls touch each other and the disc on three points situated on a circle with radius R_a [12].

3. Statistical Weibull theory

Ceramic material fractures originate at manufacturing or machining flaws, which are distributed in the material or on its surfaces. Flaws may be volume flaws (e.g. pores and inclusions) which occur during manufacturing as well as surface flaws (e.g. machining defects) which occur generally during machining. The most critical flaw (the flaw for which the most unfavorable combination of size, location, and orientation in the stress field) determines the strength of a ceramic component. Randomness in size, location and orientation of the most critical flaw is responsible for the scatter of the strength in ceramic materials. As a result, the strength varies unpredictably from component to component even if a set of nominally identical specimens are tested under the same conditions. Therefore, the strength of brittle material is not a well-defined quantity and the assessment of reliability of ceramics requires a probability approach.

Weibull derived a statistical theory of brittle fracture [25,26] for the prediction of failure probability of ceramics. His fundamental assumption is based on the weakest link hypothesis, i.e. the specimen fails, if its weakest volume element fails. The simplest form of the Weibull function [27] for uniaxial homogeneous tensile stress state for volume flaws

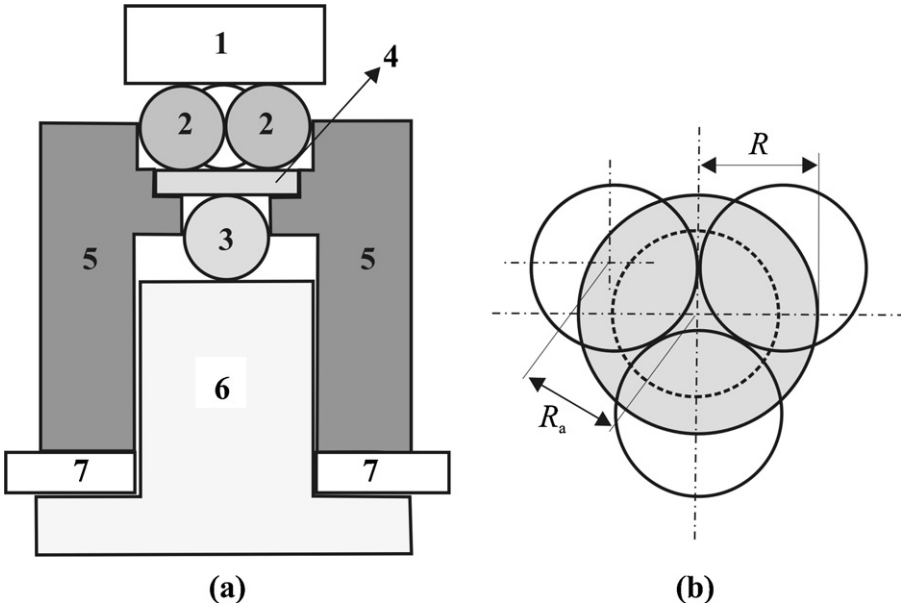

Fig. 1. (a) Sketch of the experimental setup of B3B-test and (b) ball configuration.

is given in Eq. (1):

$$P_{F,V}(\sigma, V) = 1 - \exp\left[-\frac{V}{V_0}\left(\frac{\sigma}{\sigma_0}\right)^m\right] \quad (1)$$

where $P_{F,V}(\sigma, V)$ is the failure probability of a ceramic component due to the volume flaws, V is the volume of the component, V_0 is the unit volume containing average number of volume cracks, σ is uniaxial applied stress, the Weibull modulus m is a measure for the scatter of strength data and σ_0 (characteristic strength) is the stress at which the failure probability is 63.2% for a specimen with a volume $V = V_0$. If the ceramic component fails due to surface flaws, the volume terms in Eq. (1) are replaced by surface terms as given:

$$P_{F,S}(\sigma, S) = 1 - \exp\left[-\frac{S}{S_0}\left(\frac{\sigma}{\sigma_0}\right)^m\right] \quad (2)$$

where $P_{F,S}(\sigma, S)$ is the failure probability due to surface flaws, S is the surface of the ceramic component and S_0 is the unit surface containing average number of surface cracks. In the following, all equations will be introduced for the volume flaws and they can also be considered for surface flaws.

In real applications, a multiaxial stress state occurs in the ceramic components. As a result, not only Mode-I (tension) but also Mode-II (in-plane shear) and Mode-III (anti-plane shear) fractures affect the crack propagation. Therefore, a proper account of the spatial variation in the stress triaxiality (e.g. effect of shear stresses) must be taken by using a multiaxial failure criterion [21,28,29]. Failure due to cracks subjected to mixed-mode loading is commonly expressed in terms of an equivalent Mode-I stress intensity factor $K_{I,eq}$ as [30,31]:

$$f(K_I, K_{II}, K_{III}) = f(K_{I,eq}, 0, 0) \quad (3)$$

The equivalent stress intensity factor, $K_{I,eq}$ depends on the Modes I–III stress intensity factors of the crack and, hence, on the geometry of the crack and on the multiaxial stress field. Using Eq. (3), an equivalent stress σ_{eq} can be defined

$$\sigma_{eq} = \frac{K_{I,eq}}{Y_I\sqrt{c}} \quad (4)$$

where Y_I is the geometric factor for equivalent Mode-I and c is the crack length. The equivalent stress is the uniaxial tensile stress which would have the same damaging effect as the applied multiaxial stress state [32]. The proper definition of the equivalent stress does not only depend on the type of fracture causing crack but also the fracture criterion for the multiaxial stress state. Then the uniaxial stress σ in Eq. (1) is replaced by the equivalent stress σ_{eq} as

$$P_{F,V}(\sigma_{eq}, V) = 1 - \exp\left[-\frac{1}{V_0}\int_V \frac{1}{4\pi}\int_\Omega \left(\frac{\sigma_{eq}}{\sigma_0}\right)^m d\Omega dV\right] \quad (5)$$

where Ω represents the orientation of the flaw. It is always practical to introduce an effective volume V_{eff} for the design of ceramics. Effective volume can be calculated as

$$V_{eff} = \int_V \frac{1}{4\pi}\int_\Omega g^m d\Omega dV \quad (6)$$

where g is the geometry function which characterizes the stress distribution relative to the reference stress in the component and it can be determined in Eq. (7):

$$\sigma_{eq} = \sigma^* g \quad (7)$$

where σ^* is the reference stress (e.g. maximum principal tensile stress in the component). The final form of the failure probability function can be formulated as follows:

$$P_{F,V}(\sigma^*, V_{eff}) = 1 - \exp\left[-\frac{V_{eff}}{V_0}\left(\frac{\sigma^*}{\sigma_0}\right)^m\right] \quad (8)$$

For a prescribed failure probability given in Eq. (8), the characteristic strengths $\sigma_{0,1}$ and $\sigma_{0,2}$ for two load cases with effective volumes $V_{\text{eff},1}$ and $V_{\text{eff},2}$ have a relationship as given below:

$$\left(\frac{\sigma_{0,1}}{\sigma_{0,2}}\right)_{\text{experimental}} = \left(\left(\frac{V_{\text{eff},2}}{V_{\text{eff},1}}\right)^{1/m}\right)_{\text{numerical}} \tag{9}$$

Eq. (9) explains the size effect of ceramic components (i.e. as the size of the ceramic component increases, the strength decreases) and is used for the prediction of ceramic components with different sizes.

When series of specimens are tested by B3B-test, the experimentally measured characteristic strength $\sigma_{0,\text{sample}}$ is normalized by unit volume or by unit surface in order to obtain the standardized material strength $\sigma_{0,\text{v}}$ or $\sigma_{0,\text{s}}$ as given below:

$$\begin{aligned}\sigma_{0,\text{v}} &= \sigma_{0,\text{sample}}\left[\frac{V_{\text{eff,sample}}}{V_0}\right]^{1/m}\\ \sigma_{0,\text{s}} &= \sigma_{0,\text{sample}}\left[\frac{S_{\text{eff,sample}}}{S_0}\right]^{1/m}\end{aligned} \tag{10}$$

The standardized strength value is characterized as the basic strength of a material and is independent of the component size and test type. Therefore, there is a need of a general formulation for the calculation of effective volume and effective surface of B3B-test specimens. In this article, normal stress criterion (NSC), maximum principal stress criterion (MPS) and empirical criterion of Richard (ECR) are used; these three criteria showed the greatest correlation with experimental results for alumina under tension–torsion test [23].

In MPS, the failure is governed by the maximum principal stress σ_1 [33]:

$$\sigma_{\text{eq}} = \sigma_1 \tag{11}$$

NSC is based on the assumption that crack extends in the plane perpendicular to the direction of maximum normal tensile stress regardless of the initial plane of the crack [34,35]. In NSC, the equivalent stress is taken as the normal stress σ_n acting on the crack plane:

$$\sigma_{\text{eq}} = \sigma_n \tag{12}$$

In this article, volume flaws are defined as randomly oriented penny-shaped (circular) cracks in an infinite body and surface flaws are modeled as straight through-wall cracks in an infinite half-space normal to the component surface. A typical penny-shaped (circular) crack is shown in Fig. 2(a).

The orientation of a crack can be defined by the direction of the normal of the crack plane relative to three principal axes, σ_1, σ_2, σ_3 which is described by the Euler angles θ, β, γ (see Fig. 2(b)). Since the orientation of the crack is given in unit sphere, one of the Euler angles (β) can be eliminated according to the relationship $\cos^2(\theta) + \cos^2(\beta) + \cos^2(\gamma) = 1$. As a result, the stress tensor on the area of such a penny shaped crack as a function of principal stresses σ_1, σ_2, σ_3 and Euler angles θ, γ can be written as follows:

$$\begin{bmatrix}\sigma_n\\ \tau_{\text{II}}\\ \tau_{\text{III}}\end{bmatrix} = \begin{bmatrix}\sin^2(\theta)\cos^2(\gamma) & \sin^2(\theta)\sin^2(\gamma) & \cos^2(\theta)\\ -\sin(\gamma)\cos(\gamma)\sin(\theta) & \sin(\gamma)\cos(\gamma)\sin(\theta) & 0\\ \cos^2(\gamma)\sin(\theta)\cos(\theta) & \sin^2(\gamma)\sin(\theta)\cos(\theta) & -\sin(\theta)\cos(\gamma)\end{bmatrix}\begin{bmatrix}\sigma_1\\ \sigma_2\\ \sigma_3\end{bmatrix} \tag{13}$$

where τ_{II} and τ_{III} are the shear stresses in Mode-II and Mode-III, respectively.

ECR is based on fitting a large set of experimental data obtained under multiaxial loading [36]. The equivalent stress is

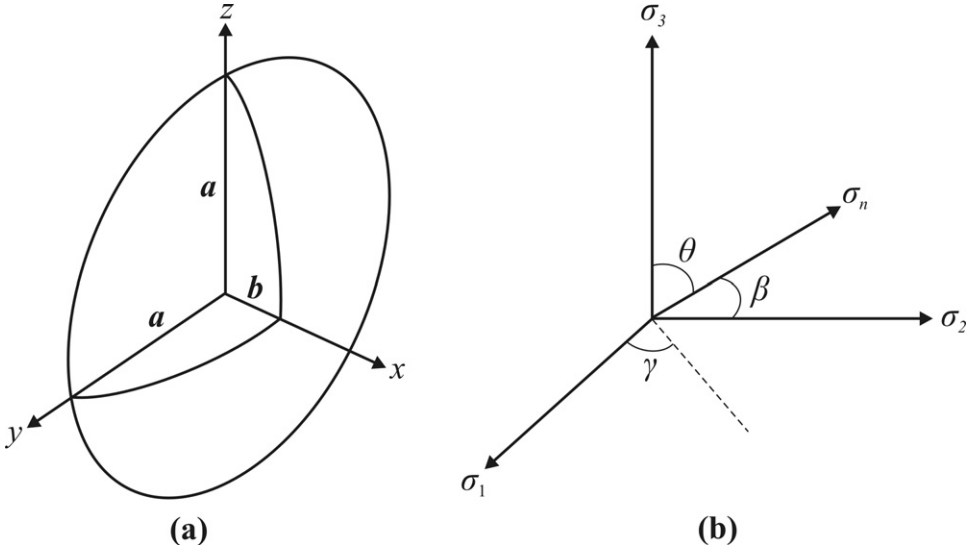

Fig. 2. (a) Representation of penny-shaped (circular) crack. (b) Representation of normal stress relative to principal axes described by Euler angles.

defined as follows:

$$\sigma_{eq} = \frac{1}{2}\left[\sigma_n + \sqrt{\sigma_n^2 + 4\tau_{II}^2\alpha_I^2\left(\frac{Y_{II}}{Y_I}\right)^2}\right] \quad \text{where} \quad \alpha_1 = \frac{K_{IC}}{K_{IIC}} \tag{14}$$

Y_I is the geometric function for Mode-I and Y_{II} is the geometric function for Mode-II. Y_I and Y_{II} for volume and surface flaws are calculated as follows:

$$\begin{aligned} &Y_I = \frac{2}{\sqrt{\pi}}, Y_{II} = \frac{4}{\sqrt{\pi}} \cdot \frac{1}{2-\upsilon} \cdot \cos(\psi) \text{ (volume flaws)} \\ &Y_I = Y_{II} = \sqrt{\pi} \cdot 1.1215 \text{ (surface flaws)} \end{aligned} \tag{15}$$

where υ is the Poisson's ratio, and ψ is the angle along the circumference of the crack with respect to the direction of the shear.

Experiments performed by different testing methods with different ceramic materials showed that α_1 gets values between 0.5 and 1.3 [37–39]. Previous studies show that the α_1 values obtained from disk specimens with chevron starter notches are smaller than asymmetric 4-point bending test. Moreover, for materials with rising R-curve, very low α_1 values were observed [39]. Since most of the ceramics (Al_2O_3 [40], ZrO_2 [41], Si_3N_4 [42]) show R-curve behavior, α_1 is used as 0.5 in this paper.

4. Finite element model

Börger et al. [11] performed numerical finite element computations and provided an analytical approximation of maximum tensile stress in B3B-test specimens. These results suggest the loading can be approximated by a simple point loading since the stress field in the disc does not depend on nonlinear changes in the loading geometry, which is primarily due to the deformation of the balls' contact with the specimen. Although using point loading can make the finite element model simpler and faster [14], large stress gradients around the loading points may appear.

In this study, in order to avoid stress gradients problems, the load is transferred on the specimen by constant pressure on the small contact area $a = 0.1t$ in all finite element computations. Fett et al. [20] performed finite element analysis of 3-ball-on-3-balls test by applying load as a constant pressure and concluded that applying pressure on a small area contact is more suitable. The finite element model of the B3B test is given in Fig. 3(a) where R is the radius of the disc, R_a is the distance between the ball contact point and the center of the disc and t is the thickness of the disc.

Finite element computations were performed by ABAQUS 6.5. The ceramic material was modeled as an isotropic elastic material. The disk was modeled by using C3D8R (An 8-node linear brick, reduced integration, hourglass control) elements and realized by a finite element net of about 70.000 elements. After global seeding, the meshes on the contact areas were refined in order to obtain more exact results. Börger et al. [11] reported the maximum tensile stress does not depend on the Young's modulus of the ceramic material. In this study, Young's modulus in the computations are taken as $E = 210$ GPa.

In Fig. 3(b), the stress distribution of a disc with $R = 10$ mm, $R_a = 8.7$ mm, $t = 2$ mm, $E = 210$ GPa and $\upsilon = 0.3$ is represented. The finite element model provided very close results (maximum 10% deviation) to the analytical approximation of maximum tensile stress provided by Börger et al. [11]. The effective volume and effective surface values are obtained by STAU Post-Processing routine [43,44] which works with the general purpose Finite Element Code ABAQUS.

5. Results and discussion

In this study, 229 numerical analyses were performed for each multiaxial failure criterion, including the parameter range: $t = 0.5$ mm, 1 mm, 2 mm; $R = 10$ mm, 20 mm; $R_a/R = 0.5$, 0.7, 0.87; $m = 10$, 12, 14, 16, 18, 20 and $\upsilon = 0.2$, 0.25, 0.3. For $R = 20$ mm, only $t = 2$ mm was considered. For some cases, in order to obtain a better parametric study, $\upsilon = 0.22$ and $\upsilon = 0.27$ was used as extra data. Therefore, totally 229 points were analyzed. The range of investigated surface area is between 660 mm^2 and 2764 mm^2 and volume is between 157 mm^3 and 2513 mm^3. For NSC and ECR, the effective volume and effective surface values, for MPS only effective volume values are calculated because, with MPS, only effective volumes can be calculated by STAU.

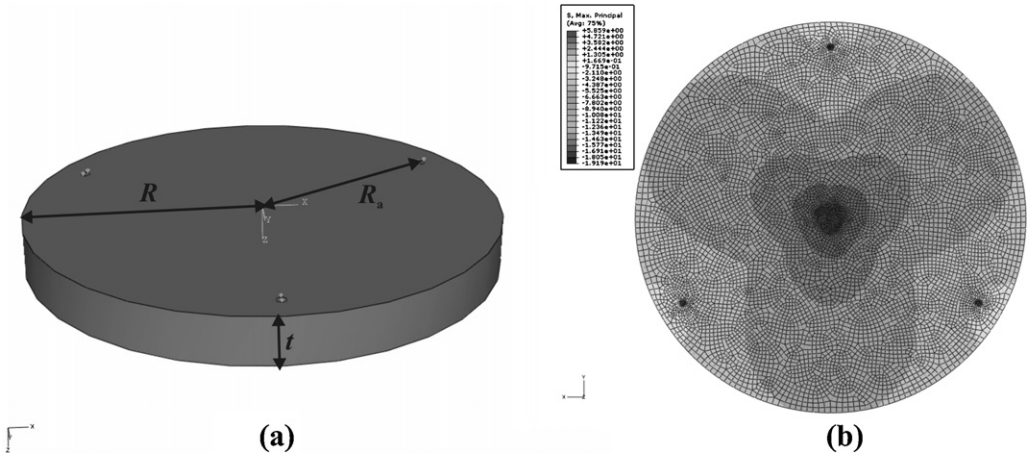

Fig. 3. (a) Finite element model of B3B test. (b) Stress distribution in B3B specimen.

One of the most frequently used criteria is the principle of independent action (PIA) where all principle stresses act independently. Since PIA criterion does not exist in STAU, MPS is used instead, due to the fact that for a material with a Weibull modulus of $m = 20$, there is only 4% deviation between PIA and MPS, and this difference is often hidden by the scatter of data [21]. For instance, Harrer et al. [19] calculated the effective volume of a Si_3N_4 specimen with $t = 2$ mm, $R = 10$ mm, $R_a/R = 0.80$, $v = 0.27$ and $m = 15.9$ as 0.065 mm^3 by using PIA and the effective volume determined with MPS in this study is 0.068 mm^3 (5% deviation with PIA). Effective volume calculated with same parameters according to NSC is equal to 0.0072 mm^3 which is much lower than PIA, as expected.

Fitting functions of effective volume/surface are determined by the stepwise regression method. Stepwise regression method is an appropriate tool to predict a fitting function when dealing with large numbers of independent variables. It is a robust tool and provides the best combination of independent variables that best fits the dependent variable with less computing [45].

The fitting functions for effective volumes and effective surfaces are given in the following form:

$$V_{\text{eff}} = V \cdot f_{\text{V}}\left(v, m, \frac{t}{R}, \frac{R_a}{R}\right)$$
$$S_{\text{eff}} = S \cdot f_{\text{S}}\left(v, m, \frac{t}{R}, \frac{R_a}{R}\right) \quad (16)$$

where V is the volume of the specimen and is equal to $V = \pi R^2 t$, S is the surface of the specimen and is equal to $S = 2\pi R^2 + 2\pi R t$ and f_{V} and f_{S} are the dimensionless fitting functions for effective volume and effective surface, respectively. The fitting functions of effective volume/surface for the considered multiaxial failure criteria are given below.

5.1. Normal stress criterion (NSC)

$$f_{\text{V}}\left(v, m, \frac{t}{R}, \frac{R_a}{R}\right) = b_0 + b_1 \cdot m + b_2 \cdot m^2 + b_3 \cdot \left(\frac{t}{R}\right)\left(\frac{R_a}{R}\right)^2 + b_4 \cdot m \cdot \left(\frac{t}{R}\right) \times \left(\frac{R_a}{R}\right) + b_5 \cdot m \cdot \left(\frac{t}{R}\right) + b_6 \cdot v \cdot \left(\frac{t}{R}\right)^2 \quad (17)$$

with $b_0 = 1.463 \times 10^{-4}$, $b_1 = -1.613 \times 10^{-5}$, $b_2 = 4.470 \times 10^{-7}$, $b_3 = 4.625 \times 10^{-4}$, $b_4 = -3.427 \times 10^{-5}$, $b_5 = 1.750 \times 10^{-5}$ and $b_6 = -1.599 \times 10^{-3}$.

$$f_{\text{S}}\left(v, m, \frac{t}{R}, \frac{R_a}{R}\right) = b_0 + b_1 \cdot m + b_2 \cdot \left(\frac{t}{R}\right)\left(\frac{R_a}{R}\right)^2 + b_3 \cdot m^2 + b_4 \cdot m \cdot \left(\frac{t}{R}\right) \times \left(\frac{R_a}{R}\right) + b_5 \cdot \left(\frac{t}{R}\right)\left(\frac{R_a}{R}\right) + b_6 \cdot v \cdot \left(\frac{t}{R}\right)^2 \quad (18)$$

with $b_0 = 7.529 \times 10^{-4}$, $b_1 = -9.860 \times 10^{-5}$, $b_2 = -1.759 \times 10^{-3}$, $b_3 = 3.129 \times 10^{-6}$, $b_4 = -2.725 \times 10^{-4}$, $b_5 = 8.342 \times 10^{-3}$ and $b_6 = -1.845 \times 10^{-2}$.

In Fig. 4, numerically calculated effective volume/surface values by ABAQUS-STAU are compared with the fitted values, obtained by using Eqs. (17) and (18). According to R-squared, the computed and the fitted values are in good agreement. Fitting function for effective surface shows a higher R-squared therefore fits the data better than for effective volume. Fitting function works for smaller effective volumes better than for larger effective volumes.

5.2. Maximum principal stress criterion (MPS)

$$f_{\text{V}}\left(v, m, \frac{t}{R}, \frac{R_a}{R}\right) = b_0 + b_1 \cdot m + b_2 \cdot \left(\frac{t}{R}\right)\left(\frac{R_a}{R}\right)^2 + b_3 \cdot m^2 + b_4 \cdot v \cdot \left(\frac{t}{R}\right) \times \left(\frac{R_a}{R}\right) + b_5 \cdot \left(\frac{t}{R}\right)\left(\frac{R_a}{R}\right) + b_6 \cdot m \cdot \left(\frac{t}{R}\right)\left(\frac{R_a}{R}\right) \quad (19)$$

with $b_0 = 7.239 \times 10^{-4}$, $b_1 = -7.460 \times 10^{-5}$, $b_2 = 9.290 \times 10^{-4}$, $b_3 = 2.142 \times 10^{-6}$, $b_4 = -4.498 \times 10^{-3}$, $b_5 = 2.173 \times 10^{-3}$ and $b_6 = -9.148 \times 10^{-5}$.

The fitting function for effective volume with MPS provided R-squared = 0.932 (see Fig. 5).

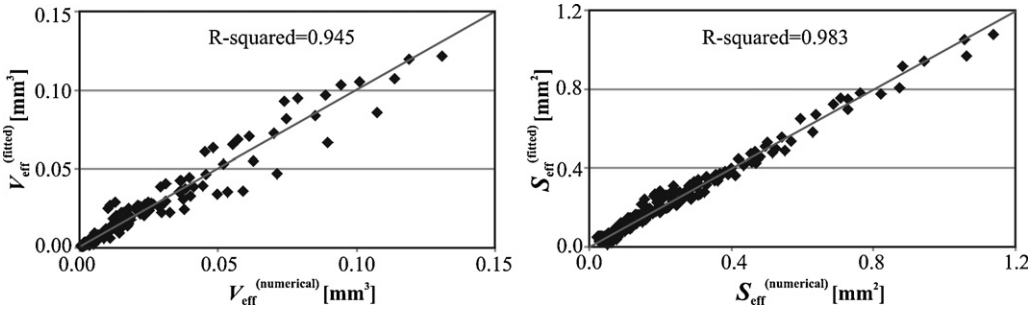

Fig. 4. Comparison of numerical (ABAQUS + STAU) effective volume and effective surface values by NSC with the results obtained from fitting functions.

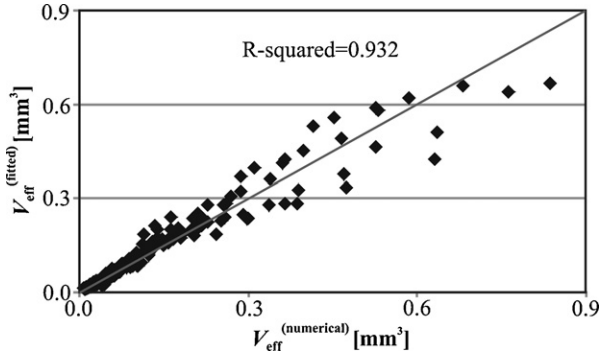

Fig. 5. Effective volumes computed numerically with MPS versus computed by fitting function.

5.3. Empirical criterion Richard (ECR)

$$f_V\left(v, m, \frac{t}{R}, \frac{R_a}{R}\right) = b_0 + b_1 \cdot m + b_2 \cdot m^2 + b_3 \cdot \left(\frac{t}{R}\right)\left(\frac{R_a}{R}\right)^2 + b_4 \cdot v + b_5 \cdot m \cdot \left(\frac{t}{R}\right)\left(\frac{R_a}{R}\right) + b_6 \cdot m \cdot \left(\frac{t}{R}\right)\left(\frac{R_a}{R}\right) + b_7 \cdot v \cdot \left(\frac{t}{R}\right)^2 \quad (20)$$

with $b_0 = 1.757 \times 10^{-4}$, $b_1 = -1.937 \times 10^{-5}$, $b_2 = 5.579 \times 10^{-7}$, $b_3 = -2.318 \times 10^{-4}$, $b_4 = -2.562 \times 10^{-5}$, $b_5 = -2.135 \times 10^{-5}$, $b_6 = 7.907 \times 10^{-4}$ and $b_7 = -2.231 \times 10^{-3}$.

$$f_S\left(v, m, \frac{t}{R}, \frac{R_a}{R}\right) = b_0 + b_1 \cdot m + b_2 \cdot \left(\frac{t}{R}\right)\left(\frac{R_a}{R}\right)^2 + b_3 \cdot m^2 + b_4 \cdot m \cdot \left(\frac{t}{R}\right) \times \left(\frac{R_a}{R}\right) + b_5 \cdot \left(\frac{t}{R}\right)\left(\frac{R_a}{R}\right) + b_6 \cdot \left(\frac{t}{R}\right)^2 + b_7 \cdot v \cdot \left(\frac{t}{R}\right) \times \left(\frac{R_a}{R}\right) \quad (21)$$

with $b_0 = 1.049 \times 10^{-3}$, $b_1 = -1.454 \times 10^{-4}$, $b_2 = -4.767 \times 10^{-3}$, $b_3 = 4.460 \times 10^{-6}$, $b_4 = -3.829 \times 10^{-4}$, $b_5 = 1.581 \times 10^{-2}$, $b_6 = -1.053 \times 10^{-2}$ and $b_7 = -4.159 \times 10^{-3}$.

Table 1
Relative mean error values between the numerical and fitted effective volume and effective surface related to NSC, MPS and ECR (Eqs. (17)–(21)).

Criterion	Effective volume Relative mean error	Effective surface Relative mean error
NSC	18.2%	15.3%
MPS	13.8%	–
ECR	17.3%	16.2%

Comparison of effective volumes and effective surfaces with the numerical values computed by ABAQUS-STAU with ECR is shown in Fig. 6. As the volume or surface becomes larger (i.e. larger dimensions, higher R_a/R ratio or lower Weibull modulus m), fitted values show more deviation from the numerical values. This deviation is more apparent for effective volumes. This is possibly due to the increase of nonlinearity as a result of increase of contact area of the loading and supporting balls. The relative mean errors between the numerically calculated effective volume/surface values and the fitted values according to NSC, MPS and ECR (Eqs. (17)–(21)) are given in Table 1. The relative mean errors were calculated by calculating the fitting error of each point by $((V_{\text{eff, numerical}} - V_{\text{eff, fitted}})/V_{\text{eff, numerical}}) \times 100$ and $((S_{\text{eff, numerical}} - S_{\text{eff, fitted}})/S_{\text{eff, numerical}}) \times 100$ and then averaging.

In Fig. 7, effective volume and effective surface values, calculated by fitting functions with different failure criteria are given as a function of Weibull modulus m for the disk with $v = 0.25$, $t/R = 0.2$ and $R_a/R = 0.87$. Effective volume values calculated with NSC and ECR are very close to each other however MPS gives almost 2 times higher effective volume values. For high Weibull modulus values, ECR and NSC result in nearly the same effective surfaces, however, as the Weibull modulus decreases, difference between ECR and NSC increases. This figure is important because with the use of this figure, reliability of ceramic springs produced from different ceramic materials can directly be predicted.

Formulations of the fitting lines shown by solid lines in Fig. 7 are given in Eq. (22). By using Eq. (22), the effective volume and effective surface values for different Weibull parameters ($m < 10$) can be predicted:

$$\begin{aligned} V_{\text{eff}}\,(\text{NSC}) &= 0.21\exp(-0.186m) \\ V_{\text{eff}}\,(\text{MPS}) &= 0.81\exp(-0.133m) \\ V_{\text{eff}}\,(\text{ECR}) &= 0.24\exp(-0.176m) \\ S_{\text{eff}}\,(\text{NSC}) &= 2.12\exp(-0.164m) \\ S_{\text{eff}}\,(\text{ECR}) &= 3.50\exp(-0.188m) \end{aligned} \quad (22)$$

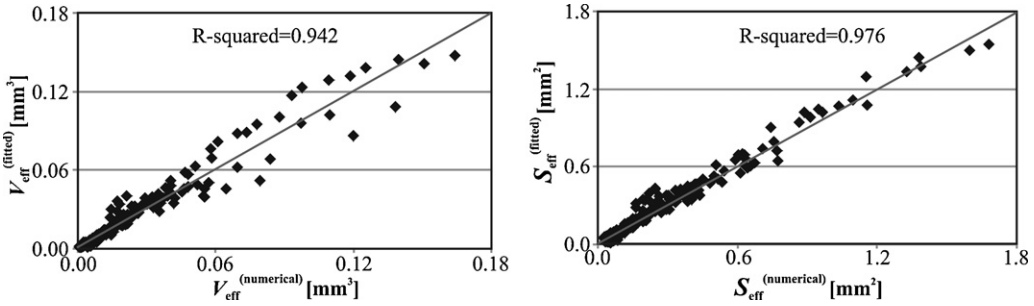

Fig. 6. Comparison of numerical (ABAQUS + STAU) effective volume and effective surface values by ECR with the results obtained from fitting functions.

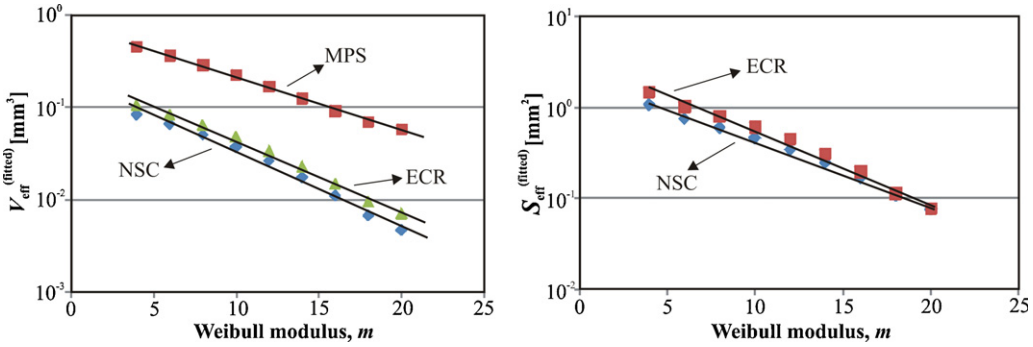

Fig. 7. Effective volumes and effective surfaces calculated by fitting functions with NSC, MPS and ECR as a function of Weibull modulus.

Size effect formulation given in Eq. (9) is mostly used for strength prediction of a ceramic component with different effective volume/surface. Here, size effect formulation is used for the verification of fitting functions and for the determination of best multiaxial failure criterion. Results of Harrer et al. [19], performed with typical commercial gas pressure sintered silicon nitride ceramics (Si_3N_4) are used for the investigation of size effect. Harrer et al. [19] tested 6 different types of specimens (for each 30 specimens) by B3B-test. The Poisson's ratio of the used material is $\nu = 0.27$ and $R_a/R = 0.80$. The dimensions and the experimentally measured Weibull parameters of the investigated samples are given in Table 2. The values in the brackets refer to the 90% confidence intervals of the Weibull parameters.

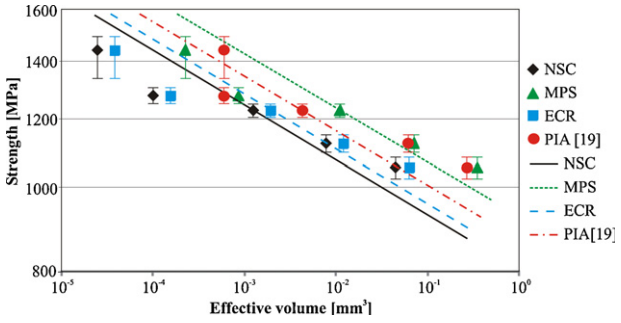

Fig. 8. Characteristic strength of Si_3N_4 specimens versus effective volume in a logarithmic plot.

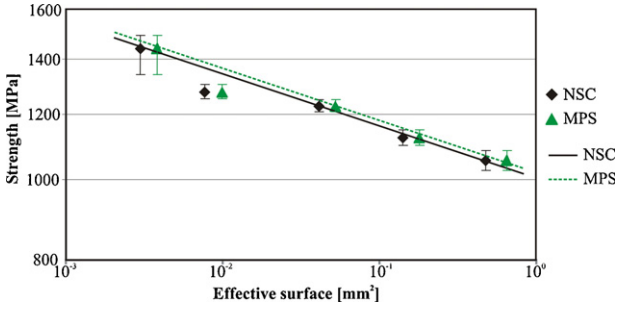

Fig. 9. Characteristic strength of Si_3N_4 specimens versus effective surface in a logarithmic plot.

Weibull modulus m shows a high scattering in Si_3N_4 samples [19] and for the following calculations, Weibull modulus is selected as an average value of $m = 16$.

Characteristic strength values are given as a function of effective volume in Fig. 8 and as a function of effective surface in Fig. 9 for different multiaxial failure criteria.

In Figs. 8 and 9, lines are created by using Eq. (9) by taking the sample 3 as reference and error bars show the 90% confidence limits of characteristic strength σ_0. Lines and the corresponding data are given with the same colors. Effective volumes calculated according to PIA are taken from the literature [19]. The strength values predicted by using effective volumes according to Weibull theory, given by lines, are out of the 90% confidence limits of characteristic strengths. However, when the effective surfaces are used in Eq. (9), the predicted strength values are mostly in the 90% confidence limits of characteristic strengths (see Fig. 9). This shows that strength prediction done by using effective surfaces gives more reliable results than by effective volumes.

For the evaluation of strength prediction performance of fitting functions for different multiaxial failure criteria, relative mean error and relative maximum error values are used (see Table 3). The relative mean error and relative maximum error is calculated as by calculating the fitting error (f_e) for each strength data by using Eq. (23) and then taking the average and maximum respectively:

$$f_e = \left(\frac{f_{\text{experimental}} - f_{\text{numerical}}}{f_{\text{experimental}}} \right) \times 100 \qquad (23)$$

$f_{\text{experimental}}$ is the experimentally measured strength value and $f_{\text{numerical}}$ is the numerically predicted strength value.

Table 2
The dimensions and the Weibull parameters (with 90% confidence intervals) of the investigated Si_3N_4 specimens [19].

Sample	Dimensions	m	σ_0
1	R = 21.5 mm, t = 2.484 mm	12.4 [9.3–15.1]	1053 [1025–1082]
2	R = 10 mm, t = 1.983 mm	15.9 [11.9–19.4]	1123 [1100–1147]
3	R = 5.4 mm, t = 1.054 mm	21.7 [16.2–26.4]	1226 [1208–1246]
4	R = 2.35 mm, t = 0.445 mm	17.7 [13.3–21.6]	1275 [1251–1300]
5	R = 1.45 mm, t = 0.291 mm	9.6 [7.2–11.7]	1437 [1388–1489]

Table 3
Relative mean error and relative maximum error values for effective volume and effective surface related to NSC, MPS, ECR and PIA.

Criterion	Effective volume		Effective surface	
	Relative mean error	Relative maximum error	Relative mean error	Relative maximum error
NSC	6.27%	12.51%	1.68%	6.76%
MPS	6.16%	12.68%	–	–
ECR	6.19%	12.56%	1.76%	6.68%
PIA [19]	6.07%	10.22%	–	–

For effective volume, PIA gives the smallest relative mean and maximum error. This means that if the effective volumes calculated according to PIA are used, more realistic strength prediction is achieved. However, the difference of relative mean error between PIA and MPS is not too high and therefore fitting functions proposed for MPS also can be used for strength prediction.

The smallest relative mean error value is obtained when effective surfaces, calculated according to NSC, are used. According to Weibull theory, strength prediction by using effective surfaces results in more accurate results. The physical interpretation of this is that the Si_3N_4 specimens fail due to surface flaws and the crack propagation occurs in the direction normal to the crack plane. Fractographic analysis performed by Harrer et al. [19] on the Si_3N_4 specimens confirms this conclusion. Harrer et al. [19] reports that surface flaws are more dangerous than volume flaws in the Si_3N_4 specimens.

6. Conclusion

In this study, fitting functions for effective volume and effective surface of B3B-test specimens were proposed for different multiaxial failure criteria. Fitting functions reveal a relative good correlation with the numerical results. Moreover, comparison with experimental results, obtained with Si_3N_4 specimens, reveals that surface flaws are strength controlling flaws for Si_3N_4 and the cracks propagate according to normal stress criterion.

For future studies, the influence of possible buckling of the disc and influence of geometric inaccuracies on effective volume and surface should be investigated. Comparison of experimental results for different ceramics (e.g. alumina, zirconia, and dental ceramics) with fitting functions would be useful to determine the most suitable failure criterion and to verify fitting functions. In addition, the effective volume and surface values of the B3B-test should be compared with other biaxial tests (e.g. ring-on-ring test, ball-on-ring test, and 3-balls-on-3-balls test), and biaxial tests providing higher effective volume and surface should be used for future strength measurements.

Acknowledgements

The author gratefully acknowledges the support on computations with piecewise regression method provided by Assoc. Prof. Dr. Abdulkadir Cevik, Gaziantep University, Civil Engineering Department. The author also would like to acknowledge De Martin, Zirve University, for her editorial contribution.

References

[1] J.H. Andreasen, Reliability-based design of ceramics, Mater. Design. 15 (1) (1994) 3–13.
[2] S. Nohut, G.A. Schneider, Failure probability of ceramic coil springs, J. Eur. Ceram. Soc. 29 (6) (2009) 1013–1019.
[3] L. Dortmans, G. de With, Weakest-link failure predictions for ceramics IV: application of mixed-mode fracture criteria for multiaxial loading, J. Eur. Ceram. Soc. 10 (2) (1992) 109–114.
[4] H. Fessler, D.C. Fricker, A theoretical analysis of the ring-on-ring loading discs, J. Am. Ceram. Soc. 67 (1984) 582–588.
[5] W. Schmitt, K. Blank, G. Schönbrunn, Experimentelle Spannungsanalyse zum Doppelringversuch, Sprechsaal 116 (1983) 397–405.
[6] U. Soltesz, H. Richter, R. Kiezler, The concentric-ring test and its application for determining the surface strength of ceramics, in: Ceramics in Clinical Applications, Elsevier Science Publishers, 1987, pp. 149–158.
[7] K.D. Shetty, A.R. Rosenfield, P. McGuire, G.K. Bansal, W.H. Duckworth, Biaxial fracture studies of a glass ceramic, J. Am. Ceram. Soc. 64 (1) (1981) 1–4.
[8] M.J. Matthewson, J.E. Field, An improved strength measurement technique for brittle materials, J. Phys. E: Sci. Instrum. 13 (1980) 355–359.
[9] A. Brückner-Foit, T. Fett, D. Munz, K. Schirmer, Discrimination of multiaxiality criteria with Brazilian disc test, J. Eur. Ceram. Soc. 17 (5) (1997) 689–696.
[10] D.J. Godfrey, S. John, Disc flexure tests for the evaluation of ceramic strength, in: Proceedings of 2nd International Conference of Ceramic Materials and Components for Engines, Deutsche Keramische Gesellschaft, Lübeck-Travemünde, (1986), pp. 657–665.
[11] A. Börger, P. Supancic, R. Danzer, The ball on three balls test for strength testing of brittle discs: stress distribution in the disc, J. Eur. Ceram. Soc. 22 (9–10) (2002) 1425–1436.
[12] A. Börger, P. Supancic, R. Danzer, The ball on three balls test for strength testing of brittle discs. Part II. Analysis of possible errors in the strength determination, J. Eur. Ceram. Soc. 24 (10–11) (2004) 2917–2928.
[13] S.M. Jeong, S.E. Park, H.L. Lee, Fracture behavior of alumina ceramics by biaxial ball-on-3-ball test, J. Eur. Ceram. Soc. 22 (7) (2002) 1129–1135.
[14] R. Danzer, P. Supancic, W. Harrer, Biaxial tensile strength test for brittle rectangular plates, J. Ceram. Soc. Jpn. 114 (11) (2006) 1054–1060.
[15] R. Danzer, W. Harrer, P. Supancic, T. Lube, Z. Wang, A. Börger, The ball on three balls test-strength and failure analysis of different materials, J. Eur. Ceram. Soc. 27 (2–3) (2007) 1481–1485.
[16] R. Danzer, T. Lube, P. Supancic, M. Damani, A. Börger, R. Binder, Austrian Patent Nr. 738/2002, 2004.
[17] R. Danzer, A. Börger, P. Supancic, R.M.A. Villanueva, Ein einfacher Festigkeitsversuch für Scheiben aus spröden Werkstoffen, Materialwiss. Werkst 34 (5) (2003) 490–498.
[18] W. Harrer, R. Danzer, P. Supancic, T. Lube, Einfluss von Kontaktspannungen auf die Festigkeit im 4-Kugelversuch, Prakt. Metallogr. 45 (1) (2008) 18–32.
[19] W. Harrer, R. Danzer, P. Supancic, T. Lube, Influence of the sample size on the results of B3B-test, Key Eng. Mater. 409 (2009) 176–184.
[20] T. Fett, G. Rizzi, E. Ernst, R. Müller, R. Oberacker, A 3-balls-on-3-balls strength test for ceramic disks, J. Eur. Ceram. Soc. 27 (1) (2007) 1–12.

[21] R. Danzer, T. Lube, P. Supancic, R. Damani, Fracture of ceramics, Adv. Eng. Mater. 10 (4) (2008) 275–298.
[22] P. Scheunemann, Discrimination of failure criteria with ceramic rings subjected to internal pressure, J. Eur. Ceram. Soc. 26 (13) (2006) 2647–2651.
[23] S. Nohut, A. Usbeck, H. Özcoban, D. Krause, G.A. Schneider, Determination of the multiaxial failure criteria for alumina ceramics under tension–torsion test, J. Eur. Ceram. Soc. 30 (16) (2010) 3339–3349.
[24] J. Lamon, Statistical approaches to failure for ceramic reliability assessment, J. Am. Ceram. Soc. 71 (2) (1988) 106–112.
[25] W. Weibull, A statistical theory of the strength of materials, Ing. Vetenskaps Akad. Handl. 151 (1939) 1–45.
[26] W. Weibull, A statistical representation of fatigue failures in solids, Trans. Royal. Inst. Technol. 27 (1949) 5–50.
[27] R. Danzer, P. Supancic, J. Pascual, T. Lube, Fracture statistics of ceramics—Weibull statistics and deviations from Weibull statistics, Eng. Fract. Mech. 74 (18) (2007) 2919–2932.
[28] S.B. Batdorf, J.G. Crose, A statistical theory for the fracture of brittle structures subjected to nonuniform polyaxial stresses, J. Appl. Mech. 41 (1974) 267–272.
[29] A.G. Evans, A general approach for the statistical analysis of multiaxial fracture, J. Am. Ceram. Soc. 61 (1978) 302–308.
[30] T. Thiemeier, A. Brückner-Foit, H. Kölker, Influence of the fracture criterion on the failure prediction of ceramics loaded in biaxial flexure, J. Am. Ceram. Soc. 74 (1) (1991) 48–52.
[31] A. Brückner-Foit, T. Fett, D. Munz, K.S. Schirmer, Discrimination of multiaxiality criteria with the Brazilian disc test, J. Eur. Ceram. Soc. 17 (5) (1997) 689–696.
[32] R. Danzer, A general strength distribution function for brittle materials, J. Eur. Ceram. Soc. 10 (6) (1992) 461–472.
[33] H. Vaughan, Crack propagation and the principal-tensile-stress criterion for mixed-mode loading, Eng. Fract. Mech. 59 (3) (1998) 377–393.
[34] F. Erdogan, G.C. Sih, On the crack extension in plates under plane loading and transverse shear, J. Basic Eng. 85 (1963) 519–527.
[35] A. Brückner-Foit, T. Fett, K.S. Schiermer, D. Munz, Discrimination of multiaxiality criteria using brittle fracture loci, J. Eur. Ceram. Soc. 16 (11) (1996) 1201–1207.
[36] H.A. Richard, M. Fulland, M. Sander, Theoretical crack path prediction, Fatig. Fract. Eng. Mater. Struct. 28 (1) (2004) 3–12.
[37] J.J. Petrovic, Mixed-mode fracture of hot pressed Si_3N_4, J. Eur. Ceram. Soc. 68 (6) (1985) 348–355.
[38] T. Fett, D. Munz, Kinked cracks and Richard fracture criterion, Int. J. Fract. 115 (4) (2002) 69–73.
[39] D. Munz, T. Fett, Ceramics—Mechanical Properties, Failure Behavior, Materials Selection, Springer-Verlag, Berlin, Heidelberg, New York, 1999
[40] M.V. Swain, *R*-curve behavior in a polycrystalline alumina material, J. Mater. Sci. Lett. 5 (1986) 1313–1315.
[41] L.R.F. Rose, M.V. Swain, Two *R*-curves for partially stabilized zirconia, J. Am. Ceram. Soc. 69 (3) (1986) 203–207.
[42] S. Fünfschilling, T. Fett, M.J. Hoffmann, R. Oberacker, T. Schwind, J. Wippler, T. Böhlke, H. Ozcoban, G.A. Schneider, P.F. Becher, J.J. Kruzic, Mechanisms of toughening in silicon nitrides: the roles of crack bridging and microstructure, Acta Mater. 59 (10) (2011) 3978–3989.
[43] A. Brückner-Foit, A. Heger, K. Heiermann, P. Hülsmeier, A. Mahler, Z. Mann, C. Ziegler, STAU 5 – User's Manual – A Post Processor for a Finite Element Program to Calculate the Failure Probability Under Thermal Shock Loading, Institut für Materialforschung II, Karlsruhe, 2005.
[44] K. Heiermann, H. Riesch-Oppermann, N. Huber, Reliability confidence intervals for ceramic components as obtained from bootstrap methods and neural Networks, Comp. Mater. Sci. 34 (1) (2005) 1–13.
[45] A. Cevik, M.T. Gogus, I.H. Guzelbey, H. Filiz, A new Formulations for longitudinally stiffened webs subjected to patch loading using stepwise regression method, Adv Eng Softw. 41 (4) (2010) 611–618.